INTERNATIONAL JOURNAL FOR NUMERICAL METHODS IN FLUIDS
Int. J. Numer. Meth. Fluids 2007; **55**:899–915
Published online 24 April 2007 in Wiley InterScience (www.interscience.wiley.com). DOI: 10.1002/fld.1501

A physically based flux limiter for QUICK calculations of advective scalar transport

Qin Qian, Heinz G. Stefan and V. R. Voller*, †

Department of Civil Engineering, St. Anthony Falls Laboratory, University of Minnesota, Minneapolis, MN 55414, U.S.A.

SUMMARY

Transient, advective transport of a contaminant into a clean domain will exhibit a moving sharp front that separates contaminated and clean regions. Due to 'numerical diffusion'—the combined effects of 'cross-wind diffusion' and 'artificial dispersion'—a numerical solution based on a first-order (upwind) treatment will smear out the sharp front. The use of higher-order schemes, e.g. QUICK (quadratic upwinding) reduces the smearing but can introduce non-physical oscillations in the solution. A common approach to reduce numerical diffusion without oscillations is to use a scheme that blends low-order and high-order approximations of the advective transport. Typically, the blending is based on a parameter that measures the local monotonicity in the predicted scalar field. In this paper, an alternative approach is proposed for use in scalar transport problems where physical bounds $C_{\text{Low}} \leqslant C \leqslant C_{\text{High}}$ on the scalar are known *a priori*. For this class of problems, the proposed scheme switches from a QUICK approximation to an upwind approximation whenever the predicted upwind nodal value falls outside of the physical range $[C_{\text{Low}}, C_{\text{High}}]$. On two-dimensional steady-state and one-dimensional transient test problems predictions obtained with the proposed scheme are essentially indistinguishable from those obtained with monotonic flux-limiter schemes. An analysis of the modified equation explains the observed performance of first- and second-order time-stepping schemes in predicting the advective transport of a step. In application to the transient two-dimensional problem of contaminate transport into a streambed, predictions obtained with the proposed flux-limiter scheme agree with those obtained with a scheme from the literature.

Received 5 December 2006; Revised 8 March 2007; Accepted 10 March 2007

KEY WORDS: flux limiter; advection transport; dissipation error; cross-wind diffusion

*Correspondence to: V. R. Voller, Department of Civil Engineering, St. Anthony Falls Laboratory, University of Minnesota, Minneapolis, MN 55414, U.S.A.
†E-mail: volle001@umn.edu

Contract/grant sponsor: National Center for Earth-surface Dynamics; contract/grant number: EAR-0120914

1. INTRODUCTION

Fate and transport of solute in the environment can often be modelled by an advection dispersion equation. For example, consider a well-mixed stream containing a contaminant at concentration $C = C_0$ flowing over an initially 'clean' sediment bed $C = 0$. The contaminant is transported into the sediment streambed by a combination of advection and dispersion processes. Advection transport is *via* flow into and through the sediment. The sediment flows can be driven by (i) pressure variations along the water–bed interface [1–3], and (ii) the longitudinal stream slope. When the stream slope S is constant and the pressure variation along the water–bed surface is induced by a periodic standing surface wave of length L and amplitude a, the dimensionless velocity field in a longitudinal section along the centreline of the stream is [2, 3]

$$\begin{aligned} u(x, y) &= -\pi \sin(2\pi x) \exp(2\pi y) + \frac{1}{2R} \\ v(x, y) &= -\pi \cos(2\pi x) \exp(2\pi y) \end{aligned} \tag{1}$$

where $R = a/LS$ is the ratio of wave steepness to streambed slope. In streambeds where the advective transport *via* (1) dominates, the change of concentration in the bed is modelled by a two-dimensional transient advection equation, in dimensionless form

$$\frac{\partial C}{\partial t} + \frac{\partial (uC)}{\partial x} + \frac{\partial (vC)}{\partial y} = 0 \tag{2}$$

The initial condition is a clean bed, $C(0 \leqslant x \leqslant 1, 0 < y \leqslant 1, t = 0) = 0$ and appropriate boundary conditions are: a Dirichlet condition $C = 1$ along the bed surface $y = 0$, a far field condition of zero concentration gradient along $y = 1$, and periodic boundary conditions along the sides $x = 0$ and 1.

A valid solution of (1) and (2) should result in the prediction of a moving sharp front separating contaminated ($C = 1$) and clean ($C = 0$) bed regions. It is well known, however, that a basic numerical solution using a first-order time and space (upwinding) approximations will predict a smeared region $0 < C < 1$ between the contaminated and clean region; this smearing can be attributed to two features:

1. In a multi-dimensional problem, the flow directions will not be aligned with the coordinate directions of the grid and the resolution into the coordinate direction results in an unphysical transport of contaminant in a direction normal to the flow. This feature, referred to as 'cross-wind diffusion', will smear out a sharp front [4].
2. The second-order derivative terms in the truncation error of the first-order approximations induce a dissipation behaviour in the solution in which sharp fronts and or pulses are 'smeared' out [5]. Note, the form of the truncation error is physically analogous to dispersion and as such this dissipation error is referred to as 'artificial dispersion'.

In the solution of a general scalar advection transport problem, both artificial dispersion and cross-wind diffusion features will be present and it is convenient to collectively refer to these features as 'numerical diffusion'. Second-order schemes for approximating the advection term e.g. QUICK [6] can dramatically reduce numerical diffusion. In such cases, however, the third-order derivatives in the leading term of the truncation error will induce spurious oscillations (dispersive errors) exhibited by a loss of local monotonicity and possible instability in the predicted solution

DOI: 10.1002/fld

[7]. An effective solution to this problem is to combine the second-order approximation for the advection term with a so-called 'flux-correction' or 'flux-limiter' scheme, e.g. [6, 8–10]. Essentially, these schemes use a measure of the local monotonicity in the predicted field to switch to a first-order (upwinding) approximation whenever and wherever non-monotonicity is identified. The effect is that the numerical diffusion, induced by the lower-order scheme, dissipates the genesis of a spurious oscillation before it can damage the quality of the solution. Well-designed flux-limiter schemes are able to produce sharp physical predictions in both steady state and transient scalar advection problems. The essential contribution of this paper is to introduce a new flux limiter that exhibits these properties. The novel and unique feature in the proposed scheme is in the criteria used for the switch from the second-order to the first-order advection approximations. As noted above, previous schemes use a measure based on the local monotonicity of the solution field. In the proposed scheme, a physical switch based on the predicted upwind values falling outside known physical limits (e.g. [0, 1] for the stream example problem) is used. It is demonstrated that, although this simple scheme sacrifices a rigorous satisfaction of monotonicity, it does produce high-quality solutions comparable to more involved monotonicity methods.

In the next section, a more detailed overview of flux-limiter methods is provided. Then the mechanics of previously reported monotonic flux-limiting schemes are outlined. This is followed by the presentation of the proposed physically based scheme. The approach is tested and its performance compared to previously reported monotonicity methods. The performance comparison includes a discussion of the role of the order of approximation used in the time stepping. The work concludes with an application of the proposed scheme to a stream-bed contamination problem along with a brief assessment of computational efficiency.

2. OVERVIEW OF FLUX-LIMITER SCHEMES

At a node point P, a control volume discretization of (2) will take the general form

$$V_p C_P^{\text{new}} = V_p C_P - \Delta t \sum_{\text{faces}} (\mathbf{u}_{\text{face}} \cdot \mathbf{n}_{\text{face}}) A_{\text{face}} C_{\text{face}} \tag{3}$$

where, with reference to Figure 1(a), V_p is the volume, Δt is the time step, A_{face} is the area of one of the control volume faces, $\mathbf{n}_{\text{face}}$ is the outward pointing normal on that face, $\mathbf{u}_{\text{face}}$ is the velocity at the face centre, and C_{face} is an approximation of the concentration on the face. Use of (3) requires the estimation of the face concentrations in terms of values at node P and its neighbours (nb). Following the work by Zalesak [8], in a general flux limiter the face concentration is estimated by a weighted average of high (H) and low (L) order approximations, i.e.

$$C_{\text{face}} = (1 - \alpha) C_{\text{face}}^{\text{L}} + \alpha C_{\text{face}}^{\text{H}} \tag{4}$$

where, depending on the scheme, the weight $0 \leqslant \alpha \leqslant 1$, can be a function of values of concentration and velocity. When trying to mitigate the effects of numerical diffusion, typical flux-limiter methods [9, 10] use weights and approximations in the general form (4) based on measures of the local monotonicity. Such methods involve local calculation spread over several node points and employ multiple schemes to ensure a smooth transition from the high- to low-order face approximation. In contrast, the alternative flux-limiter scheme developed here opts for a simpler approach, using an on/off weighting ($\alpha = 1$ or $\alpha = 0$) controlled by the single upstream nodal value falling inside or outside of the dimensionless physical range [0, 1].

DOI: 10.1002/fld

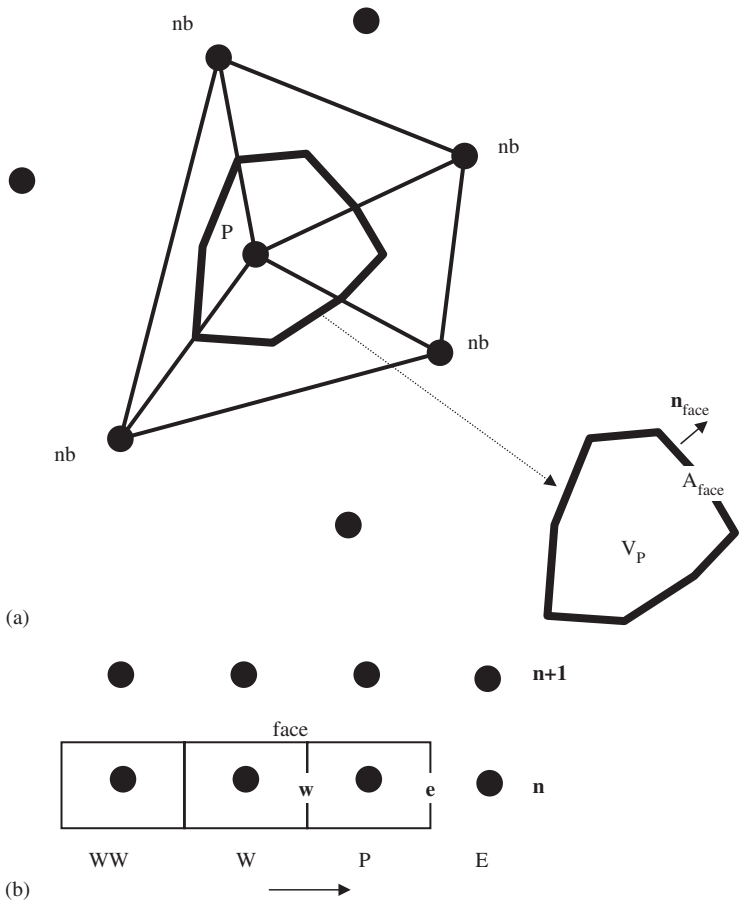

Figure 1. (a) A general control volume and (b) volumes in a one-dimensional grid.

3. EXAMPLES OF MONOTONICITY FLUX LIMITERS

The basic idea behind a monotonicity flux limiter is to (i) define a measure of the local monotonicity in the nodal scalar field and (ii) use this measure to determine the weights and approximation schemes used in the general form of (4). In this section, the mechanics of two such schemes are described: a well-established scheme SMART presented by Gaskell and Lau [9] and a recently proposed scheme from Woodfield *et al.* [10] . For simplicity, the mechanics are presented in terms of the structured one-dimensional arrangement of control volumes given in Figure 1(b); for a complete derivation and discussion of the concepts behind the methods, the reader is directed to the original references [9, 10].

3.1. The SMART scheme [*9*]

In the SMART scheme, the measure of local monotonicity is derived by comparing the gradient in C between node P and its upwind node W with the gradient between the upwind node W and

DOI: 10.1002/fld

the far-upwind node WW, i.e.

$$\gamma(P) = \frac{C_P - C_W}{C_W - C_{WW}} \tag{5}$$

A value of $\gamma<0$ indicates a change in gradient and a loss of monotonicity in C. The value of γ is used to make the following choices in (4) ($C_{\text{face}} = (1-\alpha)C^{\text{L}}_{\text{face}} + \alpha C^{\text{H}}_{\text{face}}$):

$$\alpha = \begin{cases} 0, & \gamma<0 \\ 1, & \gamma>0 \end{cases} \tag{6a}$$

$$C^{\text{L}}_{\text{face}} = C_W \tag{6b}$$

$$C^{\text{H}}_{\text{face}} = \begin{cases} C_P, & \gamma<0.2 \\ -\frac{1}{8}C_{WW} + \frac{3}{4}C_W + \frac{3}{8}C_P, & 0.2\leqslant\gamma\leqslant 5 \\ -C_{WW} - 3C_W, & 5<\gamma \end{cases} \tag{6c}$$

This scheme uses first-order upwind $C_{\text{face}} = C_W$ when monotonicity is lost ($\gamma<0$) but switches to the QUICK scheme $C_{\text{face}} = -\frac{1}{8}C_{WW} + \frac{3}{4}C_W + \frac{3}{8}C_P$—obtained by fitting a quadratic through points P, W, and WW—for most of the cases where monotonicity is present. To ensure a smooth switching to the upwind scheme and to truncate the QUICK scheme, alternative forms of $C^{\text{H}}_{\text{face}}$ are used for very small ($0<\gamma<0.2$) or large ($5<\gamma$) values of the monotonicity, as shown by the first and last components in (6c). The choice on the limits on γ are given in [9], the reader is referred to this work for full details.

3.2. The WSN scheme [*10*]

Woodfield, Suzuki and Nakabe (WSN) [10] propose an alternative scheme and demonstrate its effectiveness in solutions on unstructured meshes. In this scheme, the monotonicity measure is

$$\gamma(P) = \frac{C_I - C_{\text{min\_nb}}}{C_{\text{max\_nb}} - C_{\text{min\_nb}}} \tag{7a}$$

where I is the upwind node, $C_{\text{min\_nb}}$ is the minimum value of C in the neighbourhood of node I and $C_{\text{max\_nb}}$ is the corresponding maximum value; for the arrangement of nodes in Figure 1(b):

$$\gamma(P) = \frac{C_W - \text{MIN}(C_{WW}, C_P)}{\text{MAX}(C_{WW}, C_P) - \text{MIN}(C_{WW}, C_P)} \tag{7b}$$

DOI: 10.1002/fld

In this case, the measure is bounded, i.e. values of $\gamma>1$ and $\gamma<0$ indicate a loss of monotonicity. The value of γ is used to make the following choices in (4): $(C_{\text{face}} = (1-\alpha)C^{\text{L}}_{\text{face}} + \alpha C^{\text{H}}_{\text{face}})$

$$\alpha = \begin{cases} 0, & \gamma<0 \\ \dfrac{\gamma}{\delta}, & 0\leqslant\gamma\leqslant\delta \\ 1, & \delta<\gamma<1-\delta \\ \dfrac{1-\gamma}{\delta}, & 1-\delta\leqslant\gamma\leqslant 1 \\ 0, & 1<\gamma \end{cases} \tag{8a}$$

$$C^{\text{L}}_{\text{face}} = C_W \tag{8b}$$

$$C^{\text{H}}_{\text{face}} = -\tfrac{1}{8}C_{WW} + \tfrac{3}{4}C_W + \tfrac{3}{8}C_P \tag{8c}$$

where δ is a user defined variable, the value $\delta = 0.2$ is recommended. Unlike the SMART scheme that switches between four approximations for the face value, the WSN scheme only switches between the QUICK scheme—or a high-order equivalent on an unstructured mesh [10]—and the upwind scheme. The user-defined variable δ is used to ensure a smooth switch between the upwind and QUICK schemes; the effect of changing this value is investigated in [10].

4. A PHYSICAL FLUX LIMITER

In the streambed contamination problem in addition to maintaining monotonicity of the concentration field, a sound numerical solution should also ensure that at each node point $C_P \subset [0, 1]$ (assuming the scaling $C = C/C_0$); this feature may not be universal but could be common to a wide range of practical problems. If a numerical solver were to generate spurious oscillations, they would be exhibited by nodes where $C_P \not\subset [0, 1]$. With this in mind, for problems where obvious physical bounds on the scalar field can be identified, the following version of (4) $C_{\text{face}} = (1-\alpha)C^{\text{L}}_{\text{face}} + \alpha C^{\text{H}}_{\text{face}}$ is suggested:

$$\alpha = \begin{cases} 0, & C_W<0 \\ 1, & 0<C_W<1 \\ 0, & 1<C_W \end{cases} \tag{9a}$$

$$C^{\text{L}}_{\text{face}} = C_W \tag{9b}$$

$$C^{\text{H}}_{\text{face}} = -\tfrac{1}{8}C_{WW} + \tfrac{3}{4}C_W + \tfrac{3}{8}C_P \tag{9c}$$

Effectively the upwind scheme is switched on whenever the upwind value falls outside of the physical range $C_W \not\subset [0, 1]$. At all other faces QUICK (or a suitable unstructured alternative [10]) is used. This is a simple scheme to apply since it only uses one nodal value in the switching criterion and the switch is a simple on/off, i.e. smoothing transition zones (see (8a)) are not required. From this point on the scheme will be referred to as the physically based scheme or phib scheme.

DOI: 10.1002/fld

5. TESTING

Will such a simple scheme work? This can be determined by comparing its performance with the SMART [9] and WSN [10] monotonicity methods on a range of test problems.

5.1. Cross-wind diffusion

The cross-wind component in numerical diffusion can be isolated and studied by considering a steady state multi-dimensional problem. The classic test problem is advective transport across a box at varying angles of flow direction. The governing equation is

$$\frac{\partial(uC)}{\partial x}+\frac{\partial(vC)}{\partial y}=0 \tag{10}$$

and the boundary conditions and velocity direction are indicated in Figure 2. Part (a) of Figure 2 compares the proposed phib scheme with the WSN ($\delta=0.2$) scheme for three different flow angles, the agreement is almost exact. Both schemes show a marked improvement over the pure upwind and QUICK schemes in Figure 2(b).

5.2. Transport of a top-hat pulse

The artificial dispersion component in numerical diffusion can be isolated and studied by considering one-dimensional transient advection problems; by definition cross-wind diffusion cannot be present in one-dimensional geometry. A stringent test problem is the transport of a top-hat pulse; the governing equations are

$$\frac{\partial C}{\partial t}+u\frac{\partial C}{\partial x}=0, \quad C(0,t\geqslant 0)=0, \quad C(t=0)=\begin{cases}0, & x<11\\ 1, & 11\leqslant x\leqslant 20\\ 0, & 20<x\end{cases} \tag{11}$$

The solution is carried out for a unit velocity $u=1$ on a uniform grid with a unit spacing $\Delta x=1$. In this way, the time step Δt can be directly equated to the Courant number ($c=u\Delta t/\Delta x$). Figure 3 shows explicit first-order time-stepping results on a uniform grid of $\Delta x=1$ and $\Delta t=0.1$. The results show predictions of the concentration field obtained with the SMART, WSN ($\delta=0.2$) and phib scheme at time $t=460$ (4500 calculations steps); the analytical solution at this time is provided as a point of reference. All the schemes have a good performance transporting the pulse over a long distance without much distortion or loss. Differences between the proposed phib scheme and the alternative monotonicity schemes are very small.

5.3. Transport of a step function

A further one-dimensional transient problem—rich in performance information—is the advective transport of a step function. This problem is essentially the one-dimensional version of the stream problem; the governing equations are

$$\frac{\partial C}{\partial t}+u\frac{\partial C}{\partial x}=0, \quad C(0,t\geqslant 0)=1, \quad C(x>0,\ 0)=0 \tag{12}$$

DOI: 10.1002/fld

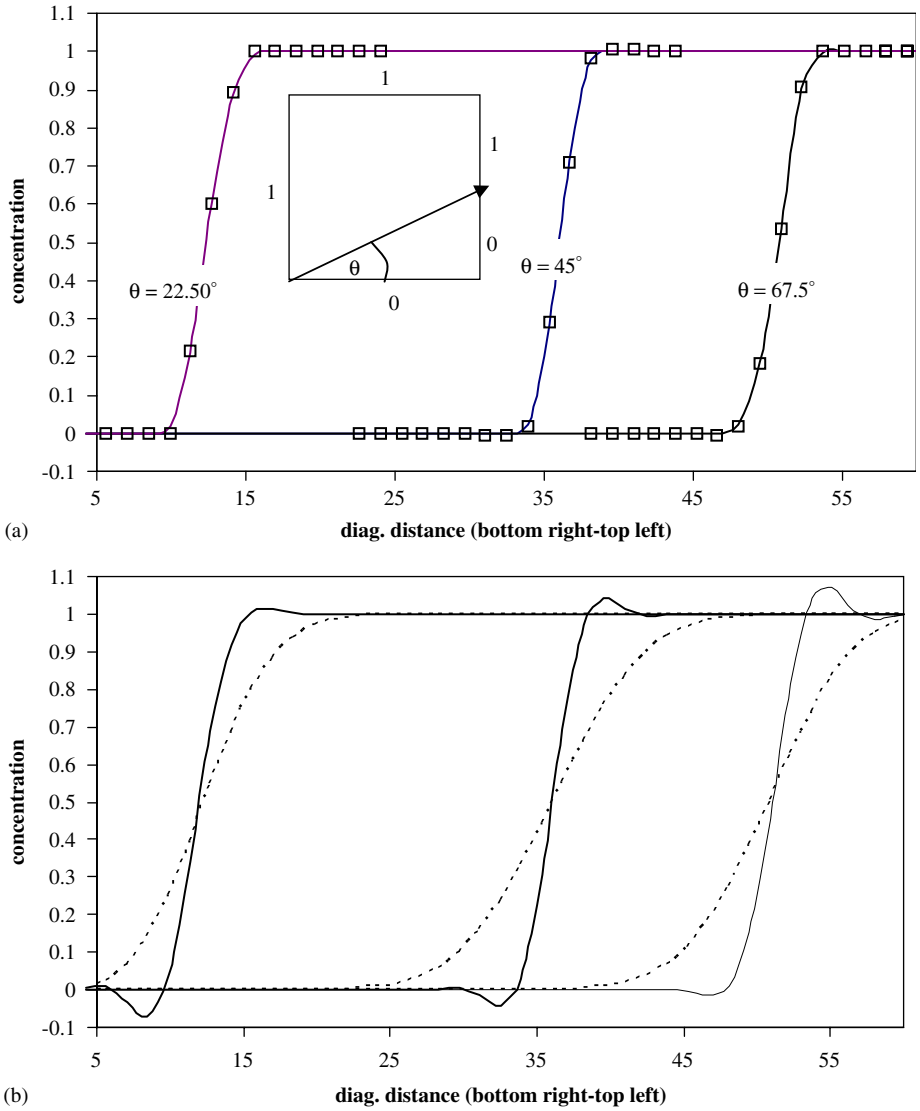

Figure 2. Cross-wind diffusion: (a) solid line WSN scheme, symbols phib scheme and (b) solid line QUICK, dashed lines upwind.

As with the top-hat pulse, the solution is obtained for a unit velocity $u = 1$ and a unit spacing $\Delta x = 1$ so that the time step Δt can be equated to the Courant number ($c = u\Delta t/\Delta x$). Figure 4 shows explicit first-order time-stepping results for $\Delta t = 0.1$ ($c = 0.1$). The results show predictions of the concentration field obtained with the SMART, WSN ($\delta = 0.2$) and the phib scheme at time $t = 450$ (4500 calculation steps); all the schemes' predictions are essentially the same. The amount of smearing in the numerical solution is spread over 2–4 cells, about 0.5% of the domain. To

DOI: 10.1002/fld

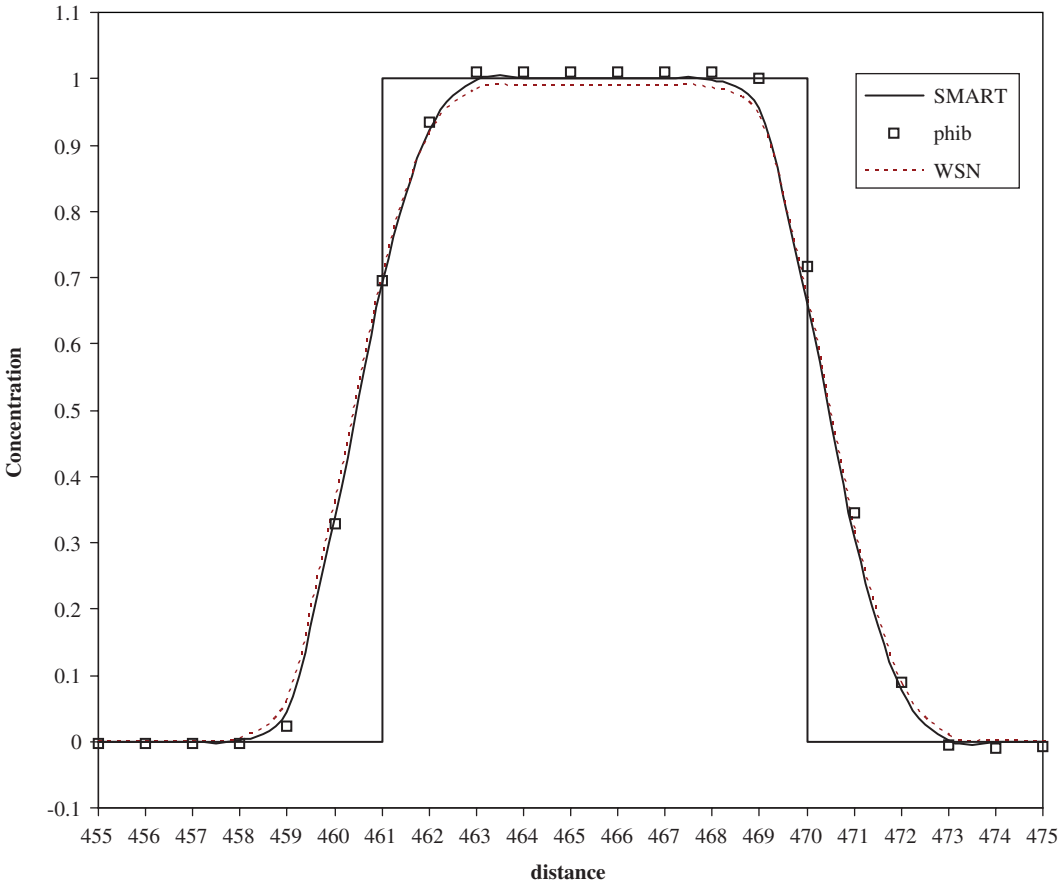

Figure 3. Advective transport of top-hat pulse, after 4500 steps and a Courant number $c = 0.1$.

indicate the need for a flux limiter the inset in Figure 4 shows the pure upwind and pure QUICK solutions at time $t = 50$ (500 calculation steps); the extensive smearing of the upwind scheme and non-physical oscillations of the QUICK scheme are very apparent.

Note an over-shoot is required to activate the phib scheme, so a small amount of non-monotonicity is inevitable. The results in Figures 3 and 4, however, clearly indicate that any non-monotonicity and resulting physical oscillations in the phib scheme are negligible.

6. TIME STEPPING

6.1. Transport of step function at larger Courant number

In the transient test problems discussed above, a relatively conservative choice of time step (Courant number) was used. When the Courant number c is increased, the performance of the schemes with a fully explicit time can deteriorate or even break down. Figure 5 shows predictions of the step advection problem after 900 calculation steps when $c = 0.5$ (a fivefold increase in the time step

DOI: 10.1002/fld

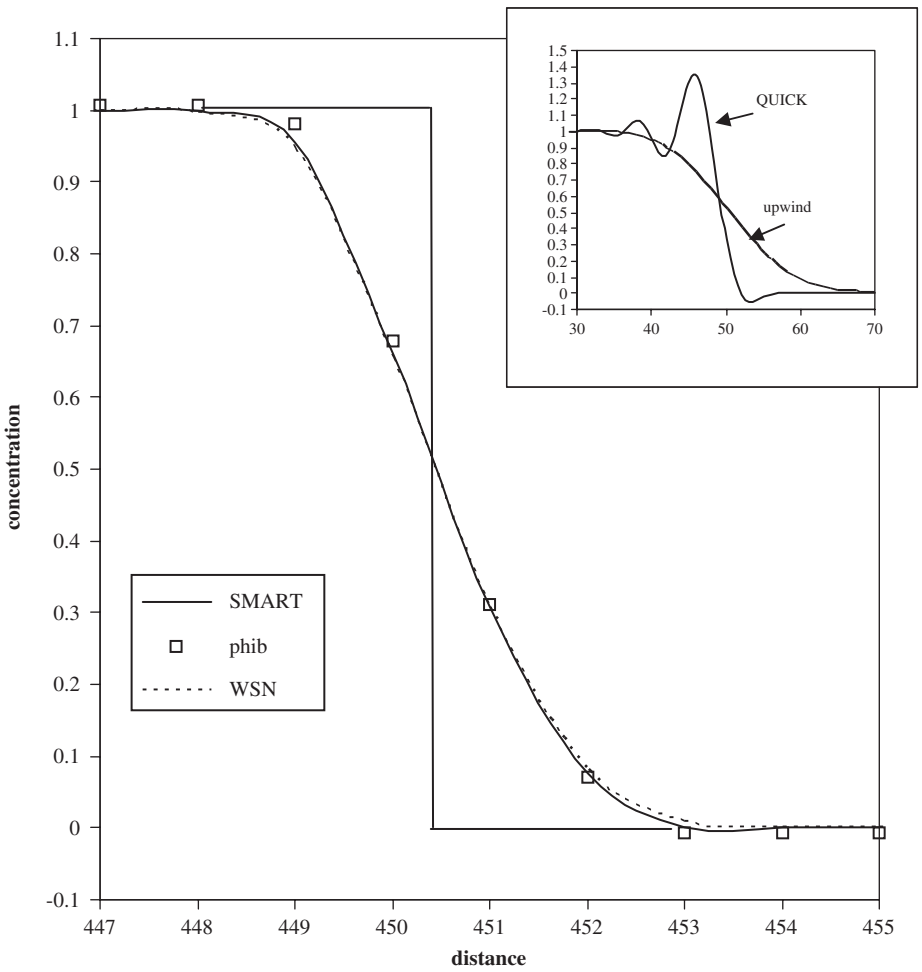

Figure 4. Advective transport of step function after 4500 steps at $c = 0.1$; inset shows upwind and QUICK solutions at early times.

used in Figure 4). When first-order time stepping is used predictions from the phib scheme (open symbols in Figure 5) indicate a consistent non-physical over- and under-shoot in the vicinity of the step. The phib scheme requires that the upwind value falls outside of the physical range [0, 1] before switching to the dissipating upwind scheme and if the Courant number c is large there is insufficient time for this non-physical value to be dissipated. Despite the appearance of non-physical values in the first-order time-stepping phib scheme, the predictions are free of oscillations. In contrast a first-order time-stepping implementation of SMART (dashed line in Figure 5) breaks down into oscillations.

6.2. Second-order time stepping

The obvious solution to the poor performance of the step advection at larger values of c is to employ a second-order time stepping. In general, this will mean formulating a Crank–Nicolson implicit

DOI: 10.1002/fld

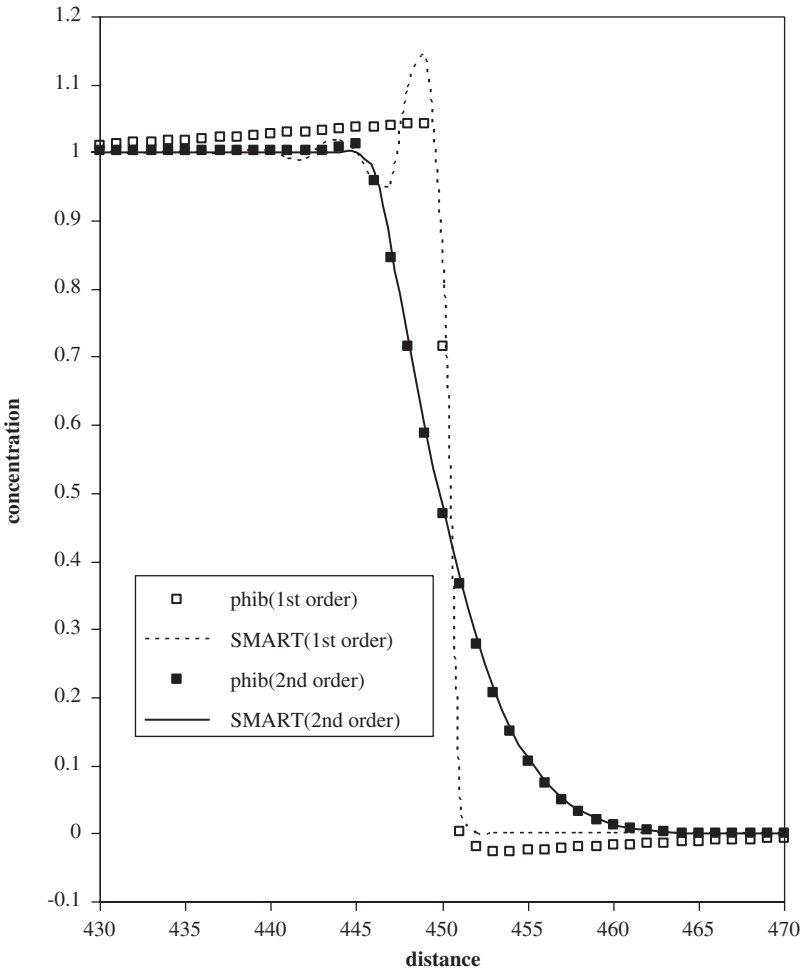

Figure 5. Advective transport of step after 900 steps with $c = 0.5$.

scheme for (12). In the case of the one-dimensional test case, however, an explicit second-order time stepping can be obtained by calculating the face values by [6]

$$C_{\text{face}} = cC_W^n + (1 - c)C_{\text{face}}^n \tag{13}$$

where C_{face}^n is the flux-limited second-order in space face approximation at the old time level n. Equation (13) can be viewed as an additional flux limiter that, depending on the value of c, 'bleeds' in enough upwinding to stabilize the chosen flux limiter. When (13) is used on the test problem it effectively removes the unphysical features in the first-order time stepping, Figure 5 shows second-order phib (solid symbols) and SMART (solid line) solutions for $c = 0.5$. For this choice of Courant number, the smoother results, however, come at the cost of a higher level of dissipation, i.e. the predicted front is significantly wider than that predicted with the first-order schemes in Figures 4 and 5.

DOI: 10.1002/fld

6.3. Analysis of the modified equation

The full nature of the performance of the first- and second-order time-stepping schemes applied to one-dimensional transport (step function) can be demonstrated by an analysis of the modified equation, i.e. the equation the finite-difference equation solves. With reference to Figure 1(b), using Taylor expansions for the concentrations at node W and E about P, and time level $n+1$ about n, the modified equation of (12) for first-order approximations in space and time is given by the right-hand side of

$$\frac{C_P^{n+1}-C_P^n}{\Delta t}+u\frac{C_P^n-C_W^n}{\Delta x}=\left.\frac{\partial C}{\partial t}\right|_P^n+u\left.\frac{\partial C}{\partial x}\right|_P^n-D\left.\frac{\partial^2 C}{\partial x^2}\right|_P^n+O(\Delta x^2+\Delta t^2) \tag{14}$$

(see Appendix A). Hence the first-order equation solves an advection–dispersion equation with grid-size-dependent diffusivity:

$$D=(1-c)\frac{u\Delta x}{2} \tag{15}$$

where $c=u\Delta t/\Delta x$ is the Courant number. In the cases where $c<1$, this term acts as an artificial dispersion and, as observed in the results (inset in Figure 4), smears out the sharp front. Progress can be made from (14) on noting that when second-order space approximations (e.g. QUICK or Central Difference) are used to approximate the concentration at the east (e) and west (w) face of the Pth control volume (Figure 1(b)) a second-order approximation for the second derivative of C at node P (see Appendix A) is

$$\frac{-C_P+C_\mathrm{e}+C_W-C_\mathrm{w}}{\Delta x}=\frac{\Delta x}{2}\frac{\partial^2 C}{\partial x^2}+O(\Delta x^2) \tag{16}$$

Adding u times this equation to (14) results in the modified equation for a second order in space and first order in time approximation of (12)

$$\frac{C_P^{n+1}-C_P^n}{\Delta t}+u\frac{C_\mathrm{e}^n-C_\mathrm{w}^n}{\Delta x}=\left.\frac{\partial C}{\partial t}\right|_P^n+u\left.\frac{\partial C}{\partial x}\right|_P^n-\left[-c\frac{u\Delta x}{2}\right]\left.\frac{\partial^2 C}{\partial x^2}\right|_P^n+O(\Delta x^2+\Delta t^2) \tag{17}$$

When flux-limiter forms are used to calculate the face concentrations the left-hand side of this equation is the finite-difference equation used in obtaining the first-order time results in Figures 4 and 5. The leading term in the truncation error now has the form of a negative diffusion. Although this feature maintains the sharp front by reducing dissipation, it also amplifies any oscillations (dispersion) that occur during the solution process. Hence, as confirmed by the results for Figures 4 and 5, sound (oscillation free) results can only be obtained with second-order space, first-order time approximations of (12) when flux limiters (SMART, WSL, phib) are employed and the Courant number is modest $c\sim 0.1$. If flux limiters are not used or c is larger (>0.25) the negative diffusion results in non-physical predictions and instability [7].

A second order in space and time approximation for (12) can be obtained by multiplying (16) by $(1-c)$:

$$(1-c)\frac{-C_P+C_\mathrm{e}+C_W-C_\mathrm{w}}{\Delta x}=(1-c)\frac{\Delta x}{2}\frac{\partial^2 C}{\partial x^2}+O(\Delta x^2) \tag{18}$$

DOI: 10.1002/fld

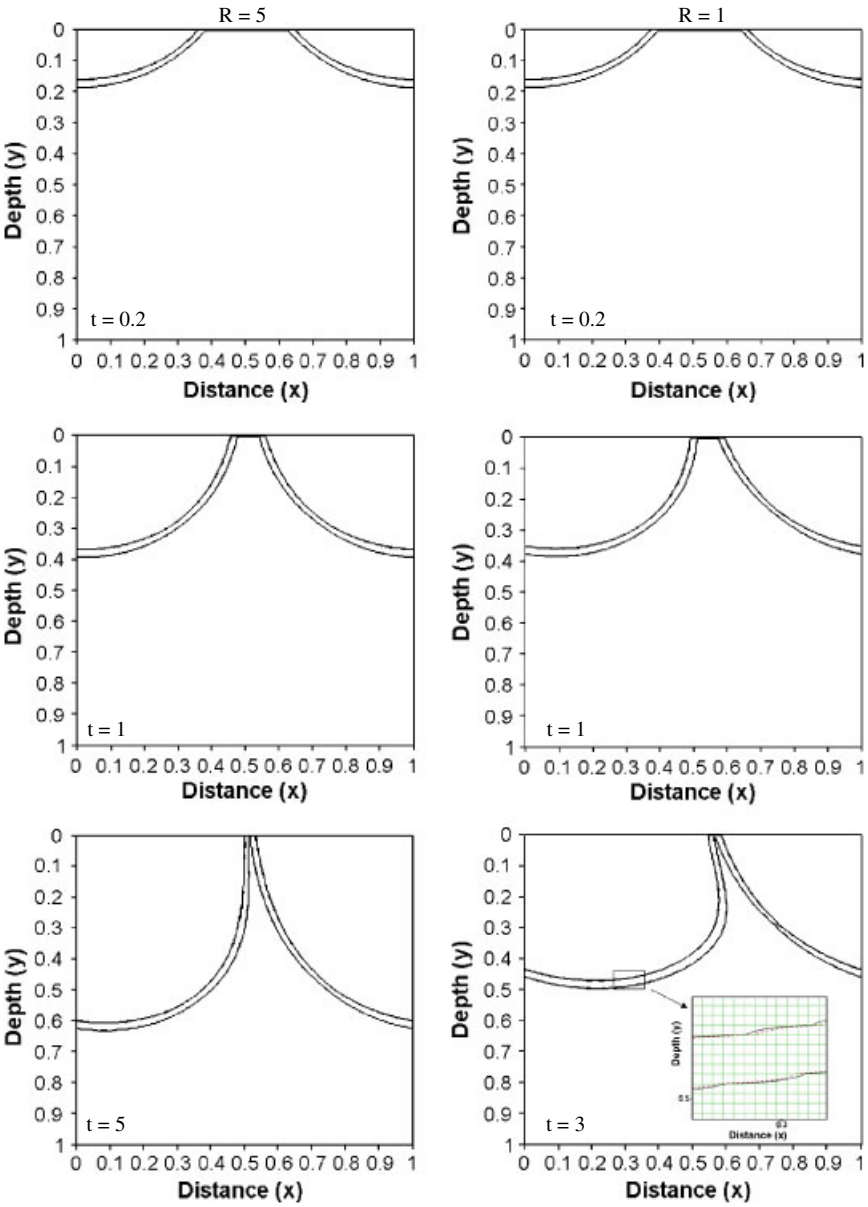

Figure 6. Results for streambed contamination. The solid line obtained by the phib scheme and dashed line obtained by the SMART scheme can hardly be distinguished.

and adding u times the result to (14)

$$\frac{C_P^{n+1} - C_P^n}{\Delta t} + u\frac{C_e - C_w}{\Delta x} = \left.\frac{\partial C}{\partial t}\right|_P^n + u\left.\frac{\partial C}{\partial x}\right|_P^n + O(\Delta x^2 + \Delta t^2) \tag{19}$$

DOI: 10.1002/fld

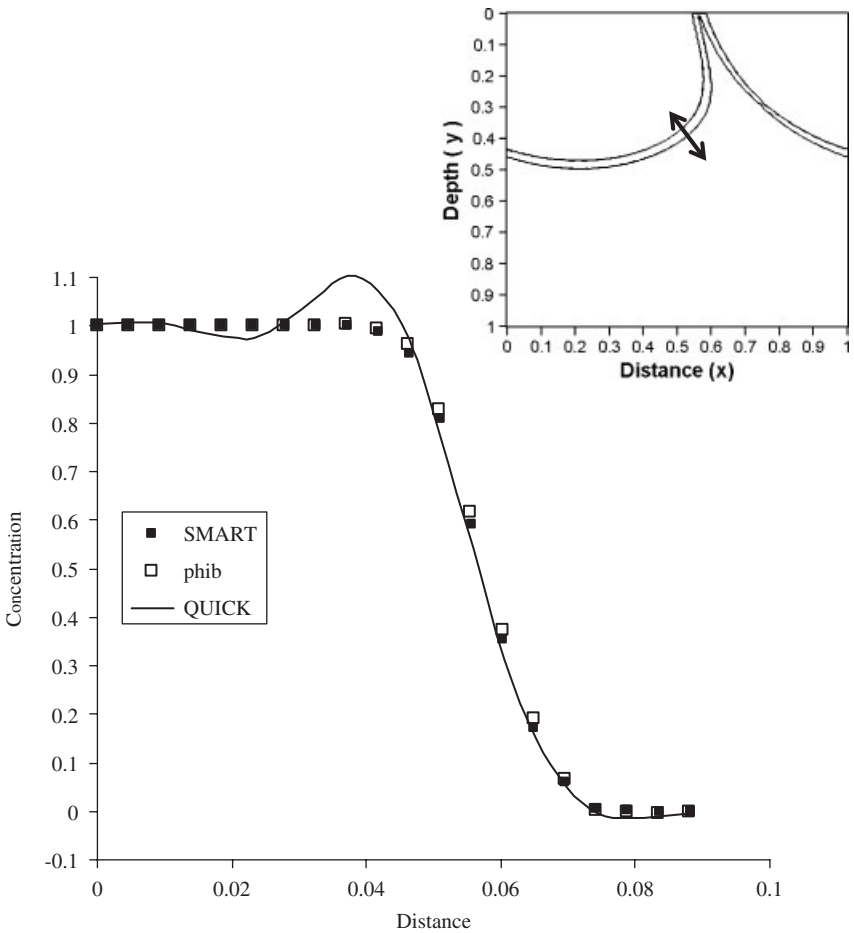

Figure 7. Profile across smeared region for $R = 5$ at $t = 3$.

where the face concentrations C_e and C_w are given by (13). The fully second-order form in (19) has no diffusion term in the truncation error. Hence, as confirmed by the fully second-order results in Figure 5, due to the loss of the negative diffusion term, predictions obtained with the scheme have less dispersion than first-order time, second-order space schemes, but more dissipation.

7. APPLICATION TO STREAMBED CONTAMINATION

The problems investigated above are somewhat idealized. It is worthwhile to see how the proposed physically based phib scheme operates on the more realistic problem of contamination of a streambed governed by Equations (1) and (2). Figure 6 shows explicit (first order in time) predictions on a square grid of size $\Delta = 0.005$ (200×200 control volume) with a time step of $\Delta t = 4 \times 10^{-5}$. The figure shows the iso-concentration lines $C = 0.99$ and 0.01 at three times,

DOI: 10.1002/fld

$t = 0.2, 1.0$ and 5.0, for two different steepness ratios, $R = 5$ and 1. The early time results are almost identical. As time increases, however, the asymmetry in the concentration filed induced by a steeper stream slope (smaller value of R) and thereby stronger flow from left to right is clearly seen. Figure 7 shows the change in solute concentration in the streambed C across the smeared region delineated by the two iso-concentration lines. The phib scheme performs very well on the stream problem. In particular, (i) the non-physical smearing in the concentration field is restricted to a narrow band, never more than $\sim$ four cells wide (see drop box in Figure 6), (ii) the profile in C across the smeared region is smooth with no under- or over-shoots (see Figure 7) and (iii) the phib and SMART predictions are in very close agreement (see drop box in Figure 6 and profile in Figure 7).

Within the context of the practical contamination problem, it is worthwhile to briefly investigate the performance of the phib scheme. In arriving at the predictions for $R = 1$ at time $t = 3$ (the right bottom panel in Figure 6) the wall clock time (to nearest minute) for the phib scheme (on a standard desktop PC) is ~ 3 min. This contrasts favourably to the wall clock time of ~ 34 min required for the author's implementation of the SMART scheme. The phib scheme can also be implemented in an implicit time-stepping solution. A fully implicit QUICK simulation of the $R = 1$ case out to time $t = 3$ (using a time step of 2×10^{-4}) takes ~ 12 min. When the phib flux limiter is implemented in this code the wall clock time increases marginally to ~ 13 min; results (concentration fields) are indistinguishable from the explicit results in Figure 6.

8. CONCLUSIONS

Low-order numerical methods for advective dominated scalar transport are well known to suffer from numerical diffusion errors that tend to smear out (dissipate) sharp gradients in the solution. Basic high-order methods may mitigate the effects of numerical diffusion but often at the cost of introducing non-physical oscillations (dispersion errors). A solution is to use the so-called flux-limiter schemes that optimize the switching between high- and low-order advection approximations to limit both dispersion and dissipation. In this paper, a new flux-limiter QUICK scheme has been introduced for application in scalar transport problems where physical limits on the scalar are known *a priori*. In contrast to previous flux limiters that employ a monotonicity measure to switch between high-order and low-order schemes the proposed scheme uses a measure based on the upwind nodal value falling outside of the known bounds on the scalar field. This switch is simple to apply and could be readily implemented into existing codes with two steps:

1. default face value to second-order face value, $C_{\text{face}} = C^{\text{2nd}}_{\text{face}}$;
2. if upwind value $C_W \not\subset [0, 1]$ reset face value to $C_{\text{face}} = C_W$.

Across a range of test problems, this simple physically based limiter 'phib' matches the performance of more involved, monotonicity-based schemes. In steady-state problems, sharp gradients are maintained when the flow is not aligned with the numerical grid. In transient problems, if the Courant number is modest $c \sim 0.1$, a first-order time-stepping implementation can transport step functions or pulses long distances without loss of shape or strength. An analysis of the modified equation provides a theoretical basis for this behaviour and also indicates why the first-order in time scheme breaks down when c is too large and why second order in time solutions show more dissipation.

DOI: 10.1002/fld

The phib scheme has also been successfully applied to the practical problem of contamination of a streambed. Results maintained a sharp front between contaminated and clean regions and were essentially identical to those obtained with a well-known and tested monotonicity scheme. These findings provide a high degree of confidence to apply the phib scheme to more general cases where dispersion in the transport cannot be neglected.

Solutions have been presented and developed on a structured grid and the QUICK scheme has been used as the high-order scheme in the flux limiter. There is reason to expect that the phib scheme would also work on an unstructured grid if an appropriate second-order scheme is used in palace of QUICK, e.g. the scheme presented by Woodfield *et al.* [10]. Further testing is required to confirm this speculation.

The bottom line is that when appropriate *a priori* physical constraints are known for a transported scalar field the proposed phib flux-limiter scheme is very easy to apply and would, based on the results shown here, be expected to produce predictions in close agreement with more involved monotonicity schemes. The key advantage of the proposed scheme is that, unlike flux limiters in the literature that use multiple switches and require several nodal values to calculate the monotonicity parameter, the phib approach uses a single on–off switch based on the single nodal upwind value. The simplicity of the phib scheme also results in a notable reduction in computation requirements. Further, the scheme can be implemented in an implicit time-stepping solution with only a small increase in computation time.

APPENDIX A: DERIVATION OF MODIFIED EQUATION

In terms of Figure 1(b), Taylor series expansions in space and time about node P can be written as

$$\begin{aligned} C_W^n &= C_P^n - \Delta x \left.\frac{\partial C}{\partial x}\right|_P^n + \frac{\Delta x^2}{2} \left.\frac{\partial^2 C}{\partial x^2}\right|_P^n + O(\Delta x^3) \\ C_P^{n+1} &= C_P^n + \Delta t \left.\frac{\partial C}{\partial t}\right|_P^n + \frac{\Delta t^2}{2} \left.\frac{\partial^2 C}{\partial t^2}\right|_P^n + O(\Delta t^3) \end{aligned} \tag{A1}$$

Rearrangement and use of the governing equation (12) to rewrite the second derivative in time as a second derivative in space leads to the finite-difference approximations

$$\begin{aligned} \left.\frac{\partial C}{\partial x}\right|_P^n &= \frac{C_P^n - C_W^n}{\Delta x} + \frac{\Delta x}{2} \left.\frac{\partial^2 C}{\partial x^2}\right|_P^n + O(\Delta x^2) \\ \left.\frac{\partial C}{\partial t}\right|_P^n &= \frac{C_P^{n+1} - C_P^n}{\Delta t} - \frac{u^2 \Delta t}{2} \left.\frac{\partial^2 C}{\partial x^2}\right|_P^n + O(\Delta t^2) \end{aligned} \tag{A2}$$

which on substitution into (12) result in the first-order modified equation (14). Further, a central difference (second-order) approximation of the second space derivative at node P is

$$\left.\frac{\partial^2 C}{\partial x^2}\right|_P = \frac{\left.\dfrac{\partial C}{\partial x}\right|_e - \left.\dfrac{\partial C}{\partial x}\right|_w}{\Delta x} + O(\Delta x^2) \tag{A3}$$

DOI: 10.1002/fld

and Taylor expansions about the faces e and w of the Pth volume give

$$\begin{aligned} C_P &= C_{\mathrm{e}} - \frac{\Delta x}{2}\left.\frac{\partial C}{\partial x}\right|_{\mathrm{e}} + O(\Delta x^2) \\ C_W &= C_{\mathrm{w}} - \frac{\Delta x}{2}\left.\frac{\partial C}{\partial x}\right|_{\mathrm{w}} + O(\Delta x^2) \end{aligned} \tag{A4}$$

Rearrangement and substitution of approximations of the first derivatives at the faces into (A3) will result in the approximation for the second derivative at node P given in (16); the truncation error in this approximation will be $O(\Delta x^2)$ provided that atleast second-order approximations are used for the face values C_{e} and C_{w}.

ACKNOWLEDGEMENTS

The authors were granted access to the computational resources of the Minnesota Supercomputing Institute for Digital Simulation and Advanced Computation at the University of Minnesota, and express their gratitude for this privilege. This work was partially supported by the STC program of the National Science Foundation *via* the National Center for Earth-surface Dynamics under the agreement Number EAR-0120914.

REFERENCES

1. Qian Q, Voller V, Stefan HG. Modeling of solute transport into sub-aqueous sediments. *Applied Mathematical Modeling* 2007; **31**:1461–1478.
2. Elliott AH, Brooks NH. Transfer of nonsorbing solutes to a streambed with bed forms: theory. *Water Resources Research* 1997; **33**:123–136.
3. Packman AI, Salehin M, Zaramella M. Hyporheic exchange with gravel beds: basic hydrodynamic interactions and bedform-induced advective flows. *Journal of Hydraulic Engineering* 2004; **130**:647–656.
4. Patankar SV. *Numerical Heat Transfer and Fluid Flow*. Hemisphere: Washington, 1980.
5. Leonard BP. The ULTIMATE conservative difference scheme applied to unsteady one-dimensional advection. *Computer Methods in Applied Mechanics and Engineering* 1991; **88**:17–74.
6. Leonard BP. A stable and accurate convective modeling procedure based on quadratic upstream interpolation. *Computer Methods in Applied Mechanics and Engineering* 1979; **19**:59–98.
7. Chen Y, Falconer RA. Advection–diffusion modelling using the modified QUICK scheme. *International Journal for Numerical Methods in Fluids* 1992; **15**:1171–1196.
8. Zalesak ST. Fully multidimensional flux-corrected transport algorithms for fluids. *Journal of Computational Physics* 1979; **31**:335–362.
9. Gaskell PH, Lau AKC. Curvature-compensated convective transport: SMART, a new boundedness preserving transport algorithm. *International Journal for Numerical Methods in Fluids* 1988; **8**:617–641.
10. Woodfield PL, Suzuki K, Nakabe K. A simple strategy for constructing bounded convection schemes for unstructured grids. *International Journal for Numerical Methods in Fluids* 2004; **46**:1007–1024.

DOI: 10.1002/fld